JEM Journal of Experimental Medicine

ARTICLE

A major role for ferroptosis in *Mycobacterium tuberculosis*–induced cell death and tissue necrosis

Eduardo P. Amaral[1], Diego L. Costa[1], Sivaranjani Namasivayam[1], Nicolas Riteau[1,2], Olena Kamenyeva[3], Lara Mittereder[1], Katrin D. Mayer-Barber[4], Bruno B. Andrade[5,6,7,8,9,10], and Alan Sher[1]

Necrotic cell death during *Mycobacterium tuberculosis* (Mtb) infection is considered host detrimental since it facilitates mycobacterial spread. Ferroptosis is a type of regulated necrosis induced by accumulation of free iron and toxic lipid peroxides. We observed that Mtb-induced macrophage necrosis is associated with reduced levels of glutathione and glutathione peroxidase-4 (Gpx4), along with increased free iron, mitochondrial superoxide, and lipid peroxidation, all of which are important hallmarks of ferroptosis. Moreover, necrotic cell death in Mtb-infected macrophage cultures was suppressed by ferrostatin-1 (Fer-1), a well-characterized ferroptosis inhibitor, as well as by iron chelation. Additional experiments in vivo revealed that pulmonary necrosis in acutely infected mice is associated with reduced Gpx4 expression as well as increased lipid peroxidation and is likewise suppressed by Fer-1 treatment. Importantly, Fer-1–treated infected animals also exhibited marked reductions in bacterial load. Together, these findings implicate ferroptosis as a major mechanism of necrosis in Mtb infection and as a target for host-directed therapy of tuberculosis.

Introduction

Tuberculosis (TB) remains a major global public health problem and is now considered the leading cause of death by a single infectious agent (World Health Organization, 2017). Progress in controlling the disease has been impeded by the lack of an effective vaccine for adult pulmonary TB and the requirement for long-term treatment with conventional antibiotics to achieve a cure. This problem has stimulated a major interest in developing new strategies for targeting *Mycobacterium tuberculosis* (Mtb) infection. An important approach, which has received considerable attention, is the design of therapies that will alter the host response to the pathogen to obtain more rapid and effective elimination of the pathogen (Wallis and Hafner, 2015).

Active TB depends on the spread of Mtb both between infected macrophages within a tissue and between organs in the case of disseminated disease. Previous studies have implicated host–cell death modality as a major factor influencing this process (Pan et al., 2005; Behar et al., 2010; Lee et al., 2011; Moraco and Kornfeld, 2014). In particular, it has been shown that Mtb growth is limited when infected macrophages undergo apoptosis, a process that contains intracellular bacteria within apoptotic bodies (Molloy et al., 1994; Oddo et al., 1998; Riendeau and Kornfeld, 2003; Martin et al., 2012). Such apoptotic cells can then be destroyed by uninfected macrophages through a process of efferocytosis (Martin et al., 2012). In direct contrast, bacterial spread is enhanced as a result of necrotic death of Mtb-infected macrophages. This outcome may stem in part from extracellular growth of bacilli released in tissues (Kaplan et al., 2003; Behar et al., 2010; Elkington et al., 2011; Amaral et al., 2016a; Lerner et al., 2017). Because of its role in bacterial dissemination as well as tissue damage, necrosis represents a potential target for intervention in the pathogenesis of TB (Pan et al., 2005; Kiran et al., 2016).

Necrotic cell death is a complex phenomenon involving a number of distinct mechanisms (Linkermann et al., 2014b; Jorgensen et al., 2017). Cells can die as a result of mechanical damage or stress ("accidental cell death") although few well-

[1]Immunobiology Section, Laboratory of Parasitic Diseases, National Institute of Allergy and Infectious Diseases, National Institutes of Health, Bethesda, MD; [2]University of Orleans and CNRS, UMR7355, Orleans, France; [3]Research Technology Branch, National Institute of Allergy and Infectious Diseases, National Institutes of Health, Bethesda, MD; [4]Inflammation and Innate Immunity Unit, Laboratory of Clinical Immunology and Microbiology, National Institute of Allergy and Infectious Diseases, National Institutes of Health Bethesda, MD; [5]Instituto Gonçalo Moniz, Fundação Oswaldo Cruz, Salvador, Bahia, Brazil; [6]Multinational Organization Network Sponsoring Translational and Epidemiological Research Initiative, José Silveira Foundation, Salvador, Brazil; [7]Wellcome Centre for Infectious Disease Research in Africa, Institute of Infectious Disease and Molecular Medicine, University of Cape Town, Cape Town, South Africa; [8]Division of Infectious Diseases, Department of Medicine, Vanderbilt University School of Medicine, Nashville, TN; [9]Universidade Salvador, Laureate University, Salvador, Bahia, Brazil; [10]Escola Bahiana de Medicina e Saúde Pública, Salvador, Bahia, Brazil.

Correspondence to Eduardo P. Amaral: eduardo.amaral@nih.gov; Alan Sher: asher@nih.gov.

defined examples of this process have been described. Instead, most forms of necrosis involve regulated pathways with specific molecular requirements. For example, pyroptotic cell death is caspase-1/11 dependent. However, previous studies have indicated that the cellular necrosis occurring in Mtb-infection is caspase-1/11 independent, arguing against the involvement of that mechanism (Lee et al., 2011; Welin et al., 2011; Wong and Jacobs, 2011; Pajuelo et al., 2018). Necroptosis is an alternative form of programmed cell death elicited through TNFR1/2 signaling that depends on the formation of a molecular complex called the necrosome, which incorporates the proteins RIPK1, RIPK3, FADD, and pro–caspase-8 (Newton et al., 2014; Pasparakis and Vandenabeele, 2015; Weinlich et al., 2017). Necroptosis is initiated by the phosphorylation of both RIP kinases and the recruitment of MLKL (Tanzer et al., 2015), which binds to cellular membranes leading to pore formation (Su et al., 2014). Previous studies have yielded contradictory findings concerning the involvement of necroptotic pathways in the necrosis induced by Mtb. Thus, macrophages from RIPK3$^{-/-}$ mice were initially described to be resistant to Mtb-induced necrosis (Zhao et al., 2017), while in two more recent studies both RIPK3- and MLKL-deficient mice were reported to display an unaltered necrotic phenotype (Stutz et al., 2018a,b).

Recently, an additional pathway of regulated necrosis, referred to as ferroptosis, has been described that, interestingly, is triggered by iron overload. The dependence of ferroptosis on iron is highly relevant to Mtb infection, which in a number of studies has been shown to be influenced by the availability of this bioactive metal. Thus, increased iron levels have been reported to be associated with elevated risk of active pulmonary TB in patients (Trousseau, 1872; Gordeuk et al., 1996; Gangaidzo et al., 2001; Boelaert et al., 2007) and augmented bacterial loads in infected mice (Lounis et al., 1999, 2001; Schaible et al., 2002). In contrast, iron chelation and mutations in host or bacterial genes affecting iron availability typically restrict pathogen growth (Schaible et al., 2002; Meyer, 2006; Owens et al., 2013; Boradia et al., 2014; Dragset et al., 2015). Moreover, Mtb infection is associated with the induction of heme oxygenase-1, a host enzyme that degrades heme to free iron in addition to carbon monoxide and biliverdin (Shiloh et al., 2008; Andrade et al., 2013; Costa et al., 2016). In the opposite direction, iron is a key component of the Fenton reaction, which generates ROSs that exhibit antibacterial effects (Lemire et al., 2013; Vilchèze et al., 2013). This evidence linking iron with the Mtb–host interaction led us to ask whether ferroptosis plays a role in the necrotic cell death and tissue necrosis triggered by Mtb infection.

In the regulated cell death associated with ferroptosis, iron overload triggers lipid peroxidation under conditions of suppressed glutathione peroxidase-4 (Gpx4) activation resulting in plasma membrane disruption (Dixon and Stockwell, 2014; Stockwell et al., 2017; Conrad et al., 2018). Ferroptosis is initiated by Fenton reaction–induced hydrogen peroxides, which upon interaction with membrane lipids produce toxic lipid peroxides. Under steady state conditions, these lipid peroxides are rapidly reduced by Gpx4 through glutathione (GSH) oxidation. However, when Gpx4 expression and/or activity is inhibited in the presence of excessive iron, lipid peroxide levels become uncontrolled and trigger necrotic cell death.

Ferroptosis can be distinguished from other forms of regulated necrosis by its association with increased iron and lipid peroxidation on the one hand and reduced GSH levels and Gpx4 activity on the other. Ferroptosis, in contrast to other forms of cell death, is blocked by lipid peroxidation inhibitors, the most widely used and best characterized of which is ferrostatin-1 (Fer-1; Dixon et al., 2012). Ferroptosis is now recognized as a major contributor in the cell death associated with a wide spectrum of diseases, including diabetes, cancer, neurodegenerative diseases, and renal failure (Stockwell et al., 2017).

In the present study, we have assessed the role of ferroptosis in the necrotic cell death occurring in macrophages infected with virulent Mtb both in vitro and in vivo. We report that Mtb-induced necrosis in the models employed is dependent on GSH, Gpx4 levels, and labile iron accumulation, as well as lipid peroxidation and, thus, fits the major criteria for ferroptosis. Importantly, we further show that blockade of the ferroptotic pathway by lipid peroxidation inhibition suppresses necrosis and leads to enhanced control of Mtb infection, suggesting a potential strategy for treating TB by targeting this necrotic cell death modality.

Results

Mtb-induced necrotic cell death in macrophages is associated with increased intracellular iron and mitochondrial superoxide levels, as well as lipid peroxidation

To examine Mtb-induced necrosis in vitro, we employed a model in which murine bone marrow–derived macrophages (BMDMs) were exposed to virulent bacteria (H37Rv strain) at different multiplicities of infection (MOIs) and cell death evaluated by using flow cytometry–based Live/Dead staining (which selectively detects cells undergoing necrosis) and lactate dehydrogenase (LDH) release 24 h and 4 d later. Following infection with H37Rv at an MOI of 5 or 10, BMDM cultures showed an elevated percentage of Live/Dead^{high} cells (Fig. S1 A and Fig. 1, A and B), as well as enhanced LDH release (Fig. 1 C) compared with uninfected cultures or macrophages infected at low MOI (MOI of 1). This Mtb-induced cell death was evident as early as day 1 and increased dramatically by day 4 post-infection (p.i.; Fig. 1, A–C). Although an increase in annexin V staining was observed in Mtb-infected cultures, it was associated predominantly with cells that were also Live/Dead positive, arguing that the cell death detected is a manifestation of necrosis rather than apoptosis (Fig. S1, B and C). In addition, consistent with previous studies, Mtb-induced macrophage necrosis in this in vitro system was found to be independent of both caspase-1 and caspase-11 (Fig. S1, D–F), arguing against the possible involvement of pyroptosis.

In Mtb infection, macrophage necrosis is typically accompanied by extracellular bacterial spread (Behar et al., 2010). Consistent with this concept, the high frequency of dead cells observed in BMDM cultures infected at high MOI (MOI of 10) was associated with a major increase in extracellular bacteria when compared with cultures exposed to Mtb at low MOI (MOI

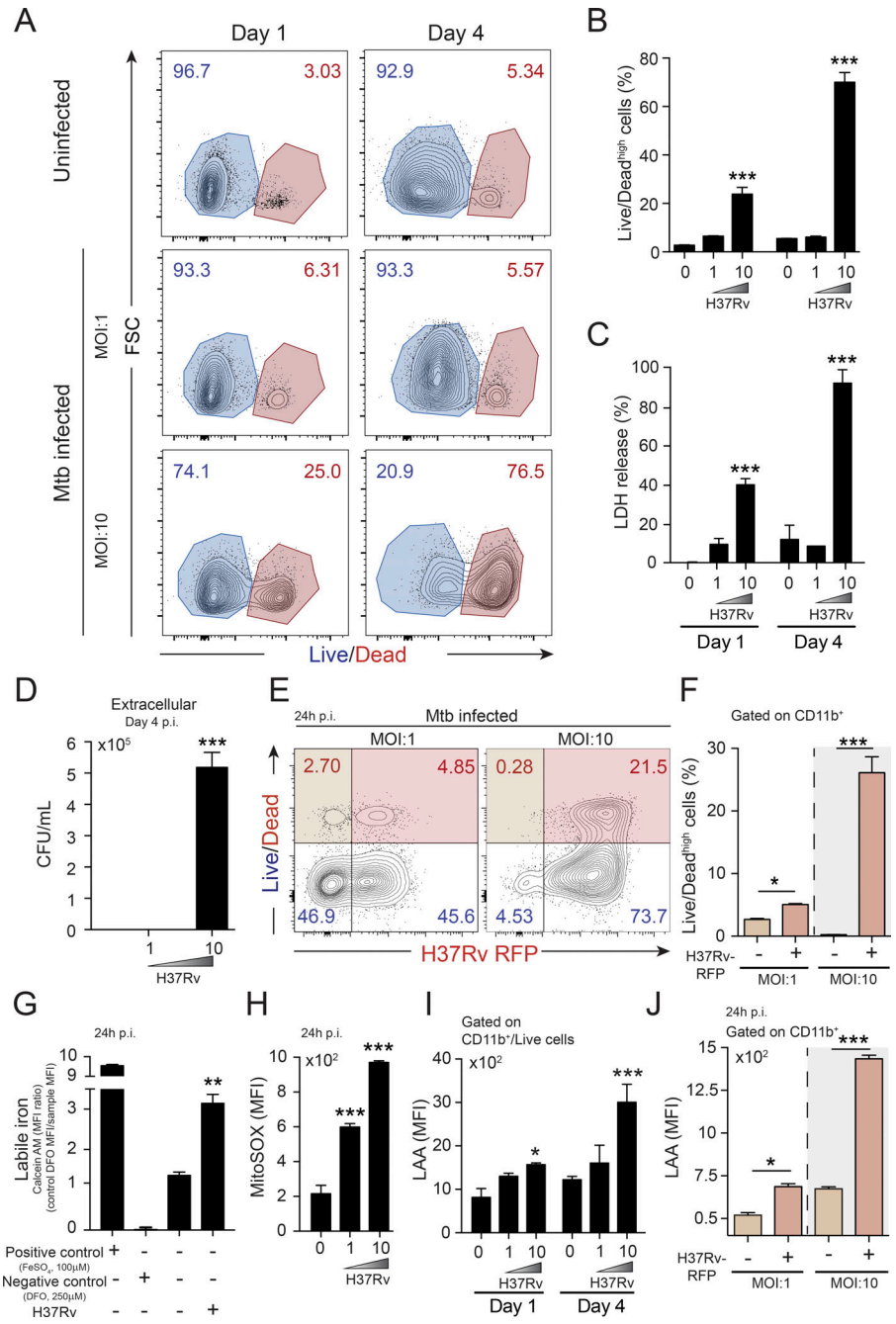

Figure 1. **Mtb triggers necrotic cell death in BMDMs by a mechanism associated with increased intracellular labile iron, mitochondrial superoxide, and lipid peroxidation.** C57BL/6 BMDMs were infected with H37Rv Mtb at different MOIs as indicated. **(A and B)** Sample FACS plots demonstrating Mtb-induced macrophage necrosis in vitro as measured by Live/Dead staining at day 1 versus day 4 p.i. and at different MOI. **(B)** Summary graph of data shown in A presenting the means ± SEM of triplicate samples analyzed. **(C)** Necrotic cell death measured by LDH released in the supernatants from the macrophage cultures shown in A and B. The data reported in A–C are representative results from at least six independent experiments performed. **(D)** The release of live mycobacteria from necrotic cells was examined by CFU quantification in macrophage culture supernatants on day 4 p.i. Results are representative of three separate experiments. **(E and F)** Necrosis of Mtb-infected macrophages was specifically assessed by using H37Rv-RFP infection and Live/Dead staining. **(F)** Summary graph of data shown in E presenting the means ± SEM of triplicate samples analyzed. **(G)** Intracellular free iron levels were assessed by calcein AM staining of macrophages at 24 h p.i. Representative data of two separate experiments are shown. **(H)** Mitochondrial superoxide was evaluated by MitoSOX staining and analyzed by flow cytometry at 24 h p.i. Results are representative of two separate experiments performed. **(I)** The kinetics of lipid peroxidation in CD11b$^+$/live cells was examined by LAA staining and analyzed by flow cytometry. Representative data from one of four independent experiments are shown. **(J)** Lipid peroxidation in H37Rv-RFP^{pos} or H37Rv-RFP^{neg} CD11b$^+$ cells was measured by flow cytometry at 24 h p.i. Results are representative of three separate experiments performed. The data shown in A–J represent the means ± SEM of triplicate samples. Statistical significance was assessed by one-way ANOVA analysis for the indicated experimental conditions (*, P < 0.05; **, P < 0.01; ***, P < 0.001). FSC, forward scatter.

of 1; Fig. 1 D). In addition, using macrophages infected with RFP-labeled H37Rv strain (H37Rv-RFP), we showed that nearly all of the cells undergoing necrosis (Live/Dead^{high} cells) also stained positively for the bacteria (Fig. 1, E and F).

We used this in vitro model of Mtb-induced macrophage death to ask whether the necrosis observed exhibits the properties classically associated with ferroptosis. Three key hallmarks of ferroptotic cell death are its dependence on intracellular iron overload, elevated ROS, and lipid peroxidation (Dixon et al., 2012). Interestingly, increased levels of intracellular labile iron (Fig. 1 G) and mitochondrial superoxide (Fig. 1 H) were both evident as early as 1 d p.i. in macrophage cultures undergoing Mtb-induced cell death. In addition, substantial elevations in membrane lipid peroxides (measured as linoleamide alkyne [LAA] levels) were observed in the same cultures (Fig. 1 I), and these increases were primarily associated with macrophages undergoing necrosis (Fig. 1 J). In Mtb-infected macrophages, the levels of lipid peroxidation positively correlated with cell death frequency, an association not observed in uninfected macrophage cultures (Fig. S2, A and B).

To further evaluate the role of iron in triggering this form of necrotic cell death, we tested the effects of iron supplementation on macrophages infected at a low MOI of 1, a setting where in the absence of added iron necrosis is usually not observed (Fig. 1 A; Divangahi et al., 2009; Lee et al., 2011). We observed a dramatic increase in Live/Dead^{high} staining (Fig. S3, A and B) and LDH

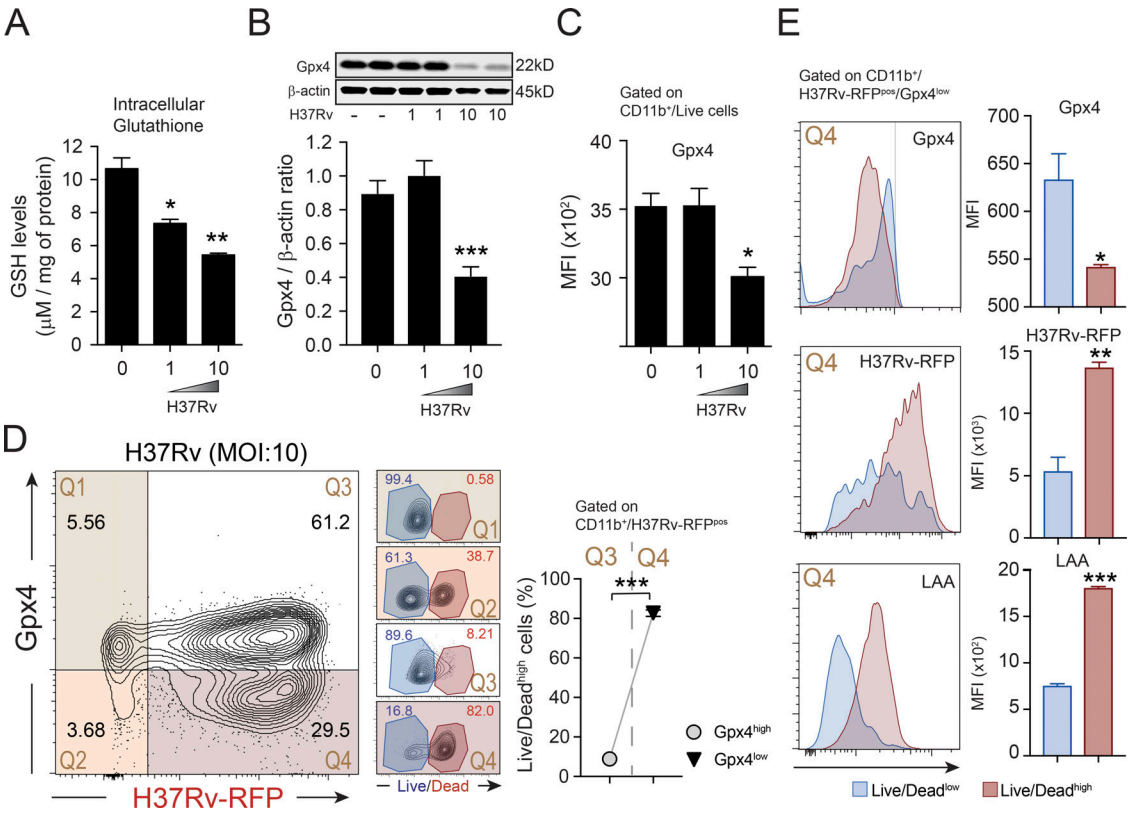

Figure 2. **Necrotic cell death of Mtb-infected macrophages is associated with reduced GSH levels and Gpx4 expression.** C57BL/6 BMDMs were infected with H37Rv Mtb at the different MOIs indicated and the following measurements performed at 24 h p.i. **(A)** Intracellular GSH levels measured in whole-cell lysates. **(B)** Intracellular Gpx4 protein levels detected by Western blotting and quantitated by densitometry. **(C)** Gpx4 expression assessed by MFI of Gpx4 staining in CD11b$^+$/live cells by flow cytometry. **(D)** Gpx4 expression (y axis) versus H37Rv-RFP (x axis; left) in infected cells was analyzed by flow cytometry. Necrotic cell death was simultaneously evaluated in the indicated gates (Q1–Q4; small insets) by Live/Dead staining (middle). Summary graph (right) of data shown in Q3 and Q4 (small insets) indicating the means ± SEM of triplicate samples analyzed. **(E)** Gpx4 expression, bacterial infection level (as measured by Mtb-RFP MFI) and lipid peroxidation in Live/Dead^{low} and Live/Dead^{high} subsets from gate Q4 (small inset) as analyzed by flow cytometry. The data shown represent the means ± SEM of triplicate samples. Significant differences are indicated with asterisks (*, P < 0.05; **, P < 0.01; ***, P < 0.001). Results are representative of three separate experiments performed for each analysis.

release (Fig. S3 C) by 24 h p.i. under conditions of iron overload, which was accompanied by elevations in mitochondrial superoxide (Fig. S3 D) and lipid peroxides (Fig. S3 E). Limited growth of the bacteria is typically observed during 24 h of culture (Fig. S4 B, left panel) arguing against a role for iron stimulation of bacterial growth (Silva-Gomes et al., 2013) as an explanation for the increase in cellular necrosis seen at this time point.

Necrotic cell death of Mtb-infected macrophages correlates with reduced levels of GSH and Gpx4 expression

The induction of ferroptosis typically depends on the suppression of Gpx4 activity due to reduced enzyme expression and/or the availability of its GSH substrate leading to uncontrolled lipid peroxidation (Ingold et al., 2018). Consistent with this concept we observed that macrophages infected with an RFP-labeled H37Rv strain at an MOI of 10 exhibited reduced levels of GSH (Fig. 2 A) and Gpx4 expression measured by Western blotting as well as by assessing mean fluorescence intensity (MFI) of the protein following intracellular staining and flow cytometry (Fig. 2, B and C). A more detailed analysis (Fig. 2, D and E) revealed that Gpx4 expression is selectively associated with the surviving cells in the Mtb-infected macrophage cultures (Fig. 2 D; gates Q3 and Q4). In addition, we observed that among the Gpx4^{low} population, the lowest expression of the enzyme was found in the cells with the strongest Live/Dead staining (Fig. 2 E). This Live/Dead^{high} population was also found to display the highest level of lipid peroxidation and to be enriched with labeled bacteria as measured by RFP MFI levels (Fig. 2 E). Together, the above observations indicate that the Mtb-induced death of macrophages in vitro exhibits the major parameters previously associated with ferroptosis.

Mtb-induced macrophage necrosis is blocked by iron chelation or by suppression of lipid peroxidation

To more directly address the involvement of ferroptosis in Mtb-induced necrosis, we tested the effects of known inhibitors and inducers of this pathway. We first assessed the dependence of macrophage necrosis on iron and found that the addition of an iron chelator, pyridoxal isonicotinoyl hydrazone (PIH), dramatically reduced cell death as measured by both Live/Dead staining (Fig. 3 A) and LDH release (Fig. 3 B) while simultaneously suppressing lipid peroxidation in the same cultures as

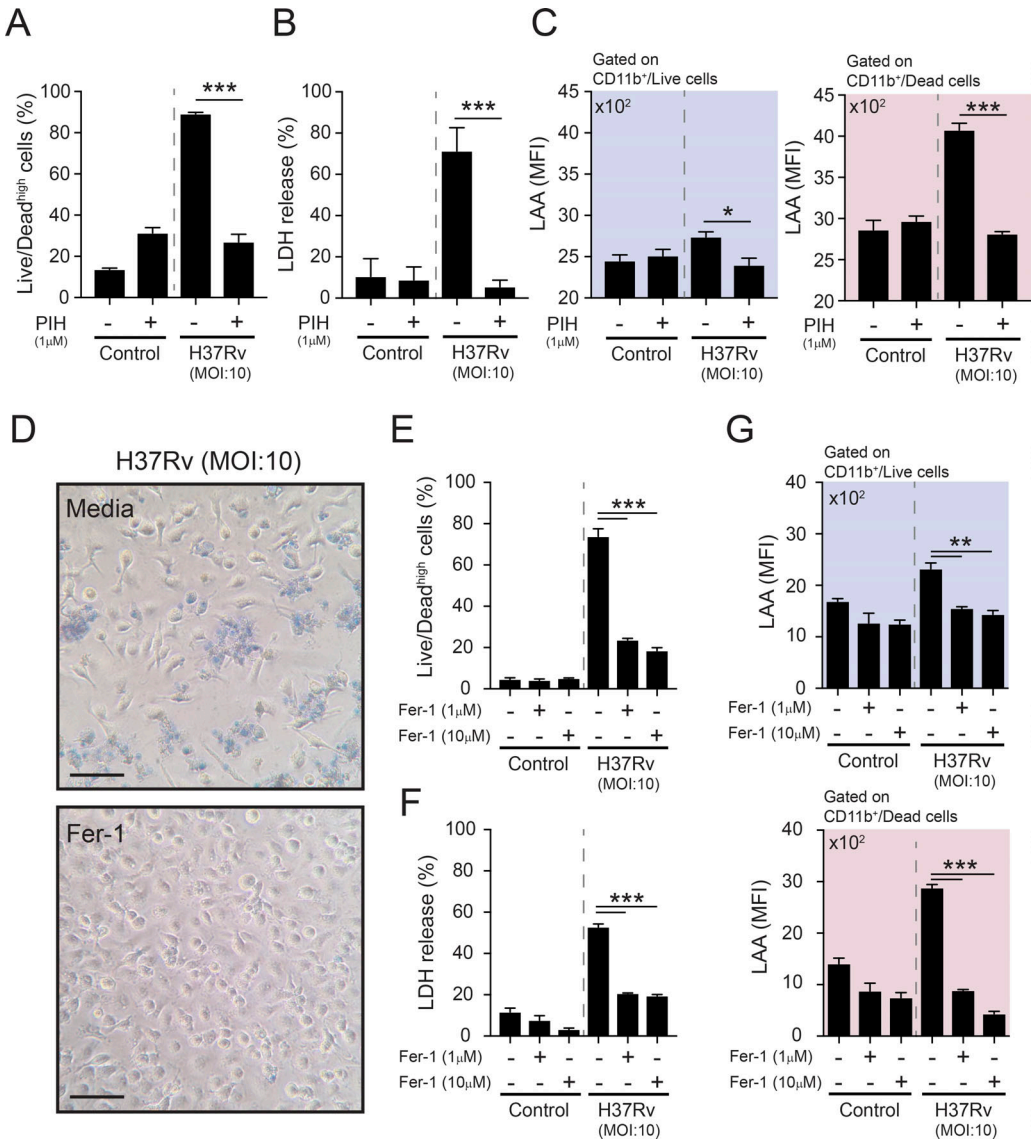

Figure 3. **Necrotic cell death of Mtb-infected macrophages is inhibited by both iron chelation and Fer-1, a well-known ferroptosis inhibitor.** C57BL/6 BMDMs were infected with H37Rv Mtb at different MOIs as indicated. **(A–C)** Macrophages were treated with the iron chelator PIH (1 μM). Cell death and lipid peroxidation were assessed on day 1 p.i. **(A)** Necrotic cell death measured by Live/Dead staining. **(B)** LDH release measured in supernatants from macrophage cultures. **(C)** Lipid peroxidation measured by LAA staining and analyzed by flow cytometry in live (left) and dead cells (right). **(D)** Representative images of infected macrophage cultures untreated (upper) or treated (bottom) with Fer-1 (10 μm) on day 4 p.i. Dead cells were evaluated by trypan blue staining (bars, 50 μm). **(E–G)** Macrophage cultures were treated with Fer-1 at the different concentrations indicated. Necrotic cell death was evaluated on day 4 p.i. **(E)** Necrosis assessed by Live/Dead staining and analyzed by flow cytometry. **(F)** LDH release measured in supernatants from macrophage cultures. **(G)** Lipid peroxidation measured by LAA staining and analyzed by flow cytometry in live (upper) and dead cells (bottom). Each data point represents the means ± SEMs of triplicate samples. Significant differences are indicated with asterisks (*, P < 0.05; **, P < 0.01; ***, P < 0.001). Results are representative of three independent experiments performed.

determined on day 4 p.i. (Fig. 3 C). Importantly, when tested at the same concentration PIH did not affect bacterial growth in liquid culture (data not shown).To directly test the requirement for lipid peroxidation in Mtb-induced necrosis, we used Fer-1, a compound that is known to block this process by reducing membrane lipid peroxides and that in prior experiments failed to display direct toxicity against cultured Mtb (Fig. S4 A). Addition of Fer-1 to macrophage cultures caused a dose-dependent inhibition in cell death (Fig. 3, D–F), an effect that, as expected, was accompanied by a reduction in lipid peroxidation (Fig. 3 G). Fer-1 also suppressed the necrosis stimulated by iron supplementation of macrophage cultures infected with Mtb at low MOI (Fig. S4, C–E), and this again was associated with reduced lipid peroxidation (Fig. S4 F). Of note, in these cultures Fer-1 addition failed to reduce bacterial burden in infected macrophages exposed to the drug for 24 h p.i. arguing against a direct toxic effect of the compound on intracellular Mtb (Fig. S4 B).

Since iron is essential for Mtb growth, it was possible that the cell death associated with iron supplementation in the above experiments was due to enhanced bacterial replication leading

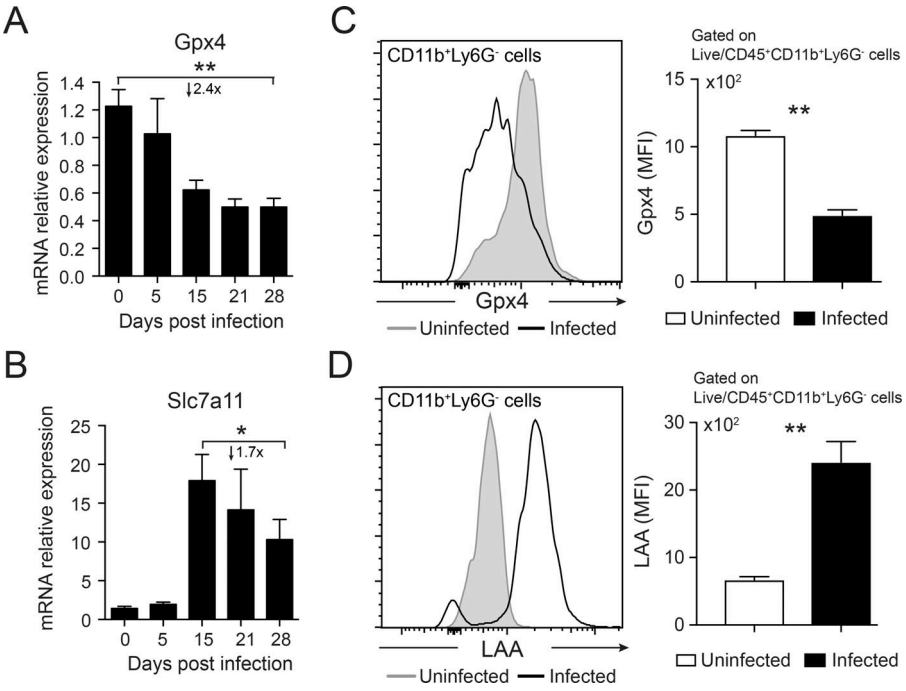

Figure 4. **Gpx4, a key regulator of ferroptosis, is down-regulated in the lung following Mtb-infection.** C57BL/6 mice were infected by intrapharyngeal inoculation with ~10^3 bacilli of Mtb (H37Rv) as a model of severe TB (n = 4–5). **(A and B)** Kinetics of *gpx4* (A) and *slc7a11* (B) mRNA expression following Mtb infection. **(C)** Gpx4 expression was measured by flow cytometric analysis in $CD11b^+Ly6G^-$ myeloid cells in the lungs of mice at 28 d p.i. **(D)** Lipid peroxidation in $CD11b^+Ly6G^-$ myeloid subset was assessed by LAA staining and analyzed by flow cytometry. The data shown represent the means ± SEM of four to five samples per experiment. Significant differences are indicated with asterisks (*, $P < 0.05$; **, $P < 0.01$). Results are representative of two independent experiments performed.

to accidental cell death rather than ferroptosis. However, as shown in Fig. S4 B (top panel), we failed to observe significant bacterial growth within the 24-h assay period. Instead, we observed an increase in extracellular bacteria that was inhibited by Fer-1 addition (Fig. S4 B, bottom panel).

Finally, to assess whether the Fer-1–inhibitable cell death mechanism observed in Mtb-infected murine macrophages also functions in human cells, we established an in vitro model of cellular necrosis using human monocyte–derived macrophages infected with H37Rv strain at an MOI of 10. As shown in Fig. S5, when examined on day 4 p.i., these infected human cells also exhibited extensive cell death, and this cellular necrosis was suppressed by Fer-1–mediated inhibition of lipid peroxidation.

In vivo Mtb infection is associated with reduced Gpx4 expression and increased lipid peroxidation

Having demonstrated a role for ferroptosis in the necrotic cell death triggered by Mtb infection of macrophages in vitro, we next asked whether the same mechanism was involved in the pulmonary necrosis induced by the pathogen in vivo. To do so, we employed a model of Mtb infection in which mice were exposed to ~10^3 bacteria (H37Rv strain) via either the intrapharyngeal or aerosol route and administered. When analyzed at 28 d p.i., lung tissue from infected mice showed a significant decrease in *gpx4* mRNA expression versus uninfected animals and beginning at 15 d p.i., a parallel increase in *slc7a11*, a transporter of the GSH precursor cysteine into the cytosol (Fig. 4, A and B). Flow cytometric analysis and staining with anti-Gpx4 antibodies of pulmonary $CD11b^+Ly6G^-$ (monocyte/macrophages) from Mtb-infected mice demonstrated a corresponding decrease in Gpx4 levels (Fig. 4 C), and these cells also displayed an increased accumulation of lipid peroxides (Fig. 4 D). In contrast, no change in Gpx4 levels was seen in $CD4^+$ T lymphocytes recovered from the same tissue (data not shown). The involvement of other cell types was not formally analyzed. Together the observed in situ cellular alterations were consistent with a ferroptotic-driven tissue necrosis mechanism.

To assess the role of lipid peroxidation Mtb infection in vivo, we measured lipid peroxide levels in the lungs of mice given either vehicle or Fer-1 (3 mg/kg) daily by intraperitoneal injection starting at 15 d p.i. (Fig. 5 A). When assayed at 28 d p.i., mice infected with Mtb displayed elevated lipid peroxidation measured in homogenates of lung tissue (Fig. 5 B). Importantly, this correlate of ferroptosis was significantly reduced in infected mice receiving Fer-1 (Fig. 5 B). Furthermore, flow cytometric analysis revealed that Mtb infection triggered increased numbers of both $CD11b^+Ly6C^+Ly6G^+$ and $CD11b^+Ly6C^+Ly6G^-$ myeloid cell populations (Fig. 5 C), as well as their lipid peroxidation levels (Fig. 5 D). Both of these alterations were markedly suppressed by treatment of the infected animals with the ferroptosis inhibitor (Fig. 5, C and D).

Mtb-induced tissue necrosis and bacterial burden are suppressed by Fer-1–mediated inhibition of ferroptosis

We next assessed the impact of ferroptosis inhibition on Mtb-induced pulmonary necrosis at the organ level. Treatment with Fer-1 caused a highly significant reduction in both lung weight and the calculated relative lung mass in infected mice (Fig. 6, A and B). Histological examination confirmed that this effect of lipid peroxidation inhibition was associated with reduced granulomatous inflammation (Fig. 6 C). To directly assess tissue necrosis, we injected mice with Sytox Green dye, which stains exposed DNA. When examined by fluorescence microscopy, whole lungs from infected mice showed extensive areas of Sytox Green staining that were not seen in the uninfected mice and that colocalized with the areas of tissue inflammation evident in the absence of the dye. Importantly,

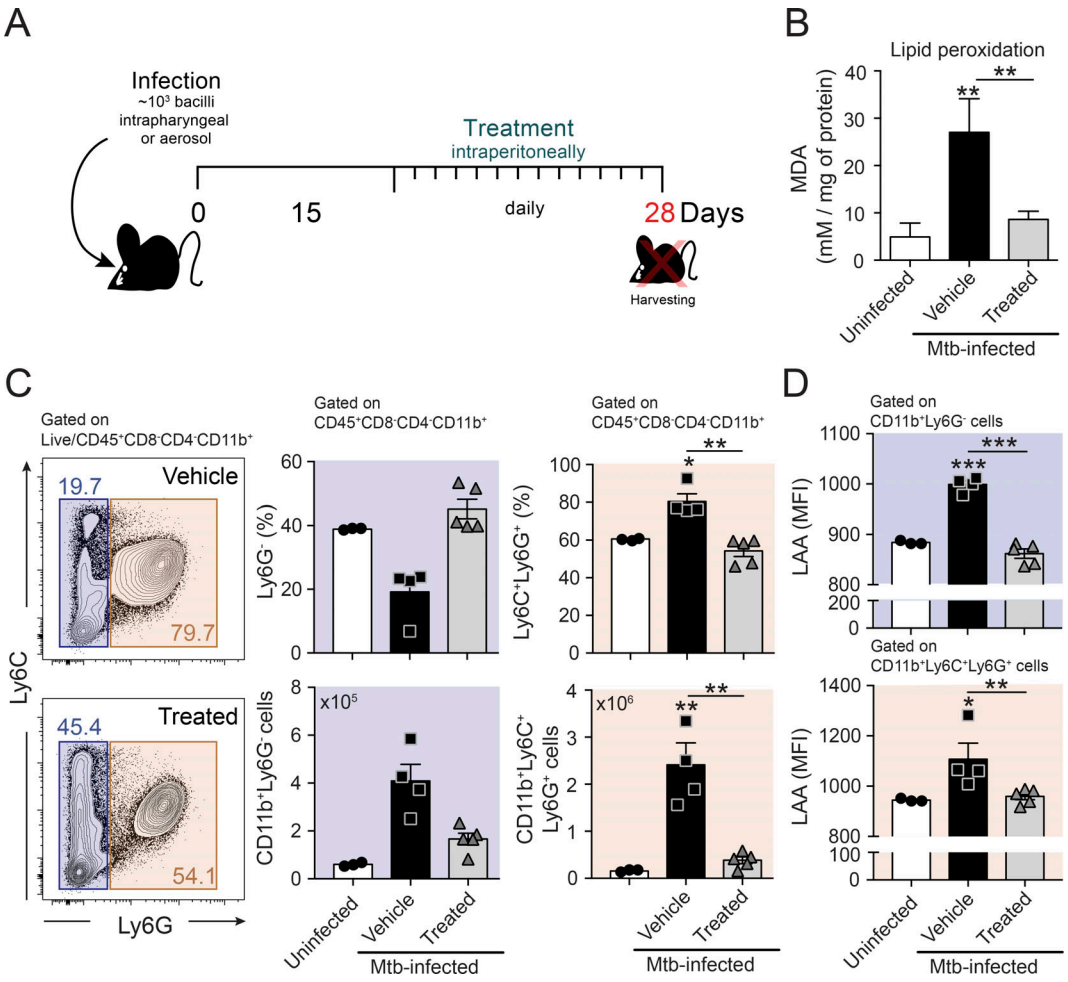

Figure 5. **Lipid peroxidation induced by Mtb in vivo is inhibited by Fer-1 treatment. (A–D)** C57BL/6 mice were infected by intrapharyngeal inoculation with ~10^3 bacilli of Mtb (H37Rv) as a model of severe TB and the animals sacrificed at 28 d p.i. Infected mice were treated daily by intraperitoneal injection with vehicle or Fer-1 (3 mg/kg/body weight) starting on day 15 p.i. (n = 4–5). **(A)** Schematic presentation of the experimental protocol. **(B)** Lipid peroxidation (malondialdehyde) measured in lung homogenates from uninfected and Mtb-infected mice. **(C)** Sample FACS plot and summary data of frequency and cell numbers of monocyte/macrophage ($CD11b^+Ly6G^-$) and neutrophil subsets ($CD11b^+Ly6C^+Ly6G^+$) in the lungs. **(D)** Lipid peroxidation in monocyte/macrophage ($CD11b^+Ly6G^-$) and neutrophil subsets ($CD11b^+Ly6C^+Ly6G^+$) in the lungs analyzed by flow cytometry. The data shown represent the means ± SEM of four to five samples per experiment. Significant differences are indicated with asterisks (*, P < 0.05; **, P < 0.01; ***, P < 0.001). The data shown are representative of three separate experiments performed.

this Sytox Green staining was markedly reduced in Mtb-infected animals treated with Fer-1 (Fig. 6 D). The above changes were also reflected in the MFI of the total lung images as well as those selectively calculated from the areas of granulomatous inflammation (Fig. 6, E and F). The latter finding suggested that the effects of Fer-1 are restricted to the sites of Mtb infection.

Finally, measurement of Mtb CFU in the lungs of the Fer-1–treated mice revealed a marked and highly significant reduction in bacterial load of >1 log (mean, 1.2) in the multiple experiments performed (Fig. 6 G). A similar reduction in CFU was evident in spleens of the same animals consistent with an effect of Fer-1 inhibition of cellular necrosis on bacterial dissemination (Fig. 6 H). The previously noted decrease in neutrophils in the lungs of Fer-1–treated animals (Fig. 5 C) is also consistent with this lowered bacterial burden.

Discussion

As an intracellular pathogen, the fate of Mtb during infection is heavily influenced by both the viability of the phagocytes in which the bacteria reside and the death modality of these host cells. There is general agreement that necrosis of infected macrophages by releasing Mtb into the extracellular milieu facilitates spread of the organism to the neighboring lung tissue, as well as its dissemination to other organs (Divangahi et al., 2013; Dorhoi and Kaufmann, 2016). Since most well-characterized forms of cellular necrosis depend on regulated cell death mechanisms involving host signaling pathways, these represent potential targets for therapeutic intervention. In the present study, we have uncovered an important role for ferroptosis, a recently described mechanism of regulated necrosis, in the fate of experimental Mtb infection both in vitro and in vivo. Since iron overload is an important trigger of ferroptosis and under certain conditions is known to promote TB, we reasoned that

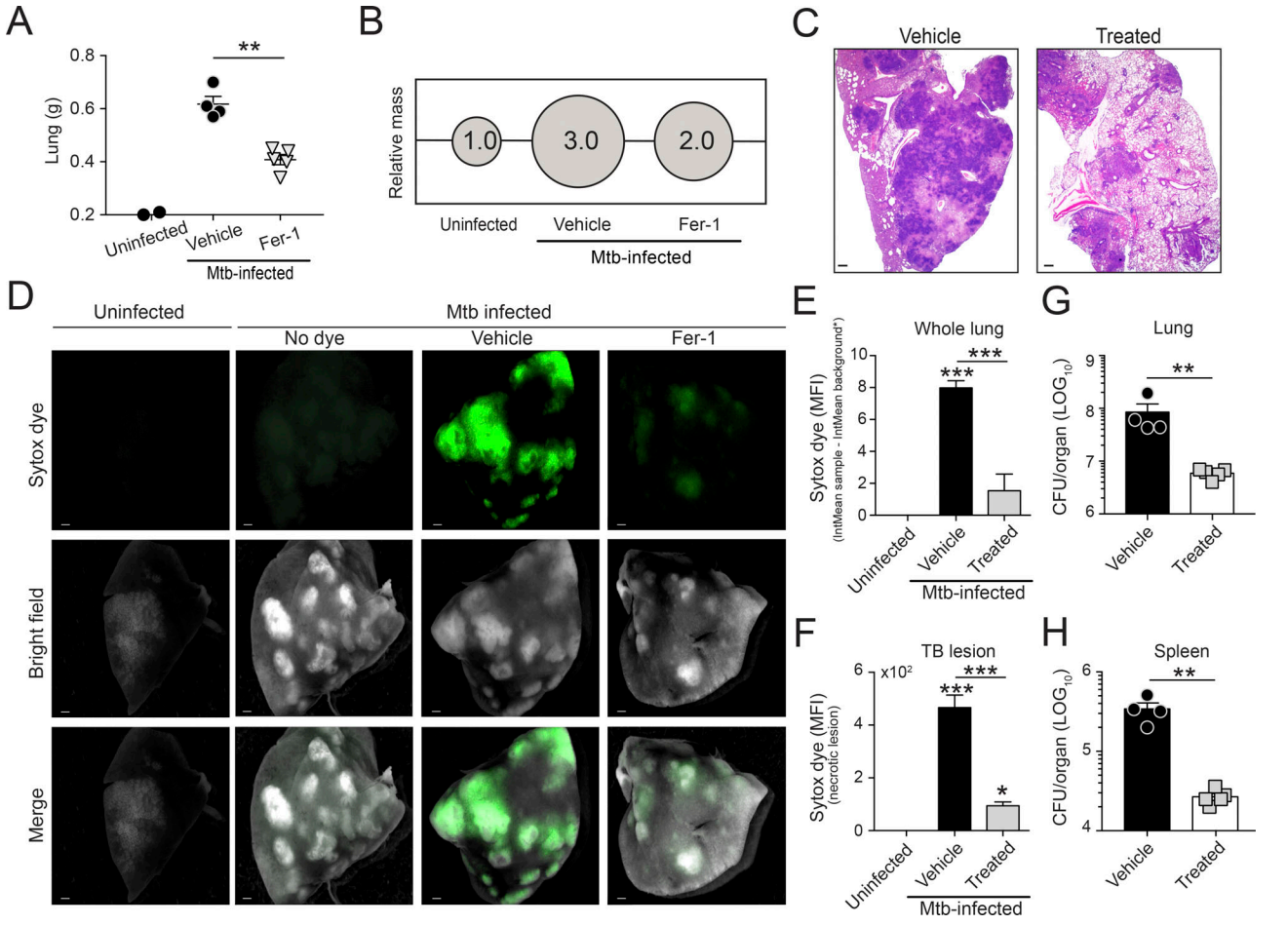

Figure 6. **Fer-1 treatment reduces lung pathology and CFU burden in Mtb-infected mice. (A–H)** C57BL/6 mice were infected by intrapharyngeal inoculation with ~10^3 bacilli of Mtb (H37Rv) as a model of severe TB and the animals sacrificed at 28 d p.i. Infected mice were treated daily by intraperitoneal injection with vehicle or Fer-1 (3 mg/kg/body weight) starting on day 15 p.i. (n = 4–5). **(A–C)** Lung weight (A), lung mass (B), and representative H&E image of merged lung sections from vehicle versus Fer-1–treated mice (C; bars, 250 µm). Each image is a composite of sections from three individual mice. The data are representative of three separate experiments performed. **(D–F)** Lung necrosis evaluated by Sytox Green DNA staining. **(D)** Representative bright-field versus fluorescence and merged images (bars, 500 µm) of whole-lung lobes from uninfected, infected, and infected Fer-1–treated mice either uninjected or injected with Sytox Green 20 min before euthanasia. **(E and F)** MFI of Sytox Green staining in whole-lung samples from five mice (E) or of individual TB lesions in these animals (F). The data are representative of two separate experiments performed. **(G and H)** Pulmonary (G) and splenic (H) bacterial loads in mice untreated and treated with Fer-1 at 28 d p.i. (n = 4–5). The data are representative of three separate experiments performed. The data shown represent the means ± SEM of four to five samples per experiment. Significant differences are indicated with asterisks (*, P < 0.05; **, P < 0.01; ***, P < 0.001).

there might be an association between this cell death modality and Mtb-induced disease.

Regulated necrosis is now viewed as a complex phenomenon involving multiple pathways in addition to ferroptosis and most prominently those associated with pyroptosis and necroptosis. Previous published studies, as well as our own current data on necrotic cell death in Mtb infection, have argued against a role for pyroptosis based on the caspase-1/11 independence of that process (Lee et al., 2011; Welin et al., 2011; Pajuelo et al., 2018; Fig. S1, D–F), while, as discussed above, the involvement of necroptosis is currently controversial (Zhao et al., 2017; Stutz et al., 2018a,b). The data presented here systematically address the role of the key elements of ferroptosis in Mtb-induced cell death both in vitro and in vivo in an animal model of severe TB. Most importantly, our findings demonstrate that Mtb-infected macrophages undergoing necrosis display an increase in lipid peroxides and that Fer-1 simultaneously blocks this accumulation, as well as cell death.

The requirement for lipid peroxide generation and accumulation is a unique feature of ferroptosis, and many of the remaining criteria delineating this form of regulated cell death are associated with that process. These include iron overload, which triggers the generation of free radicals important for the initial oxidation of plasma membrane lipids, and reduced levels of both GSH and Gpx4, which normally prevent the accumulation of toxic lipid peroxides through their biochemical reduction (Stockwell et al., 2017). As shown here, Mtb-induced necrosis of macrophages in vitro is strongly promoted by iron supplementation and inhibited by the iron chelator PIH, a compound previously shown to prevent hydroxyl radical generation by the Fenton reaction (Hermes-Lima et al., 1999, 2000; Chen et al., 2018). Furthermore, Mtb-induced cell death was found to be

associated with reduced levels of GSH and decreased Gpx4 expression. Interestingly, ROS, which is a product of Mtb-infected macrophages, has also been shown previously to influence the ferroptotic process through its involvement in the Fenton reaction (Dixon et al., 2012; Dixon and Stockwell, 2014) or potentially via an indirect effect on GSH metabolism by activation of Nrf-2 (Harvey et al., 2009; Dixon and Stockwell, 2014; Deshmukh et al., 2017). The possible contribution of ROS to the cell death pathway delineated here is currently under study.

In addition to establishing ferroptosis as a major mechanism of Mtb-induced cell death in vitro, our findings provide evidence supporting the involvement of this pathway in the pulmonary necrosis induced by the pathogen in vivo. Thus, the necrotic tissue damage in the lungs of Mtb-infected mice was shown to be associated with reduced Gpx4 levels, as well as increased lipid peroxidation, and was suppressed by treatment of the animals with the ferroptosis inhibitor Fer-1.

Although clearly pointing to a prominent role for ferroptosis in cellular necrosis in Mtb infection, our findings do not formally exclude intersections with other cell death pathways. One such intersection was recently described between ferroptosis and pyroptosis in a model of cecal ligation and puncture sepsis (Kang et al., 2018). In this study, Gpx4-inhibitable lipid peroxidation was shown to negatively regulate caspase-1/11 and gasdermin D–dependent pyroptosis, thereby protecting challenged animals from sepsis (Kang et al., 2018). Whether elements of this pathway function in Mtb-induced macrophage necrosis is currently unclear although the caspase-1/11 independence of cell death in our in vitro model argues against a major role for such crosstalk in Mtb infection. Previous studies have demonstrated that Mtb is a potent stimulus for macrophage autophagy, which is induced rapidly after infection and has been proposed to protect host cells against mycobacteria by promoting intracellular pathogen killing (Gutierrez et al., 2004; Castillo et al., 2012). Interestingly, in a different cellular model, autophagy has been shown to promote ferroptosis through degradation of ferritin (ferritinophagy; Mancias et al., 2014; Hou et al., 2016), raising the possibility that the autophagic process induced by Mtb under appropriate conditions could serve as an inductive stimulus for ferroptotic macrophage death. The recently published finding that ferritin deficiency promotes Mtb-induced pulmonary pathology is consistent with such a mechanism (Reddy et al., 2018). These potential intersections between ferroptosis and other regulated cellular processes triggered by Mtb infection will be of interest to investigate in future studies. In addition, it will be important to confirm that the role for ferroptosis revealed here in the investigation of necrosis induced by higher infection doses also applies to other situations of Mtb-induced necrosis, such as those induced by hypervirulent bacterial strains or by conventional Mtb strains in highly susceptible experimental hosts.

A further important question raised by our findings generated in a murine Mtb infection model concerns their applicability to human TB. Although this issue has yet to be formally addressed, several biomarkers of the ferroptotic response have been documented in plasma samples from Mtb-infected individuals, such as reduced GSH levels and increased accumulation of lipid peroxides (Venketaraman et al., 2008; Amaral et al., 2016b). More systematic studies assaying these, as well as additional correlates of ferroptosis in both plasma and necrotic tissue from TB patients, are needed to extend and validate the above initial observations.

Ferroptosis has now been implicated as a pathogenic mechanism in a wide variety of inflammatory conditions and in many of these situations has been considered a target for therapeutic intervention (Stockwell et al., 2017). In addition, the induction of ferroptosis by suppressing GSH generation has been proposed as a strategy for promoting the death of malignant cells (Toyokuni et al., 2017). The studies reported here raise the question of whether targeted inhibition of ferroptosis might be an approach for treatment of TB. Indeed, our data demonstrate that the lipid peroxidation inhibitor Fer-1 not only reduces pulmonary necrosis but also induces a highly significant decrease in bacterial load in both lungs and spleen of infected mice. We hypothesize that the latter effect is due to the inhibition of bacterial dissemination and spread resulting from the suppression of necrotic cell death. The alternative possibility that Fer-1 directly affects the viability of the mycobacteria themselves is unlikely based on the absence of microbicidal activity observed in both bacterial liquid cultures and in vitro infected macrophages. Nevertheless, at this stage it is impossible to rule out secondary effects of Fer-1 on other aspects of the host cellular response to Mtb that would indirectly affect tissue necrosis.

Fer-1 is extensively used as an inhibitor of ferroptosis due to its highly effective suppression of lipid peroxidation that is attributable, in part, to its antioxidant activity (Dixon et al., 2012). In addition, newer generations of the drug are under development that have been reported to display enhanced potency and stability in vivo (Linkermann et al., 2014a; Skouta et al., 2014). Interestingly, a number of other antioxidants possess ferroptosis-inhibitory properties including vitamin E, a dietary supplement that has been shown in several studies to improve TB treatment outcome when administrated adjunctively with conventional antibiotic therapy (Hernández et al., 2008; Seyedrezazadeh et al., 2008). These observations raise the question of whether Fer-1 or its newer derivatives may possess similar or more potent activity against human TB than vitamin E and conversely whether vitamin E could be used as a ferroptosis inhibitor should the former drugs prove unacceptable for clinical use in this setting. As an alternative strategy, ferroptosis can also be suppressed by augmenting Gpx4 expression and/or activity. This effect can be achieved through the administration of the trace element selenium (Ingold et al., 2018), which, interestingly, has also been shown to adjunctively enhance the outcome of conventional TB therapy when administered as a nutritional supplement (Seyedrezazadeh et al., 2008). Clearly, further preclinical studies are required to validate ferroptosis as a viable target for host-directed therapy of active TB. The potential to simultaneously lessen tissue damage while reducing pathogen burden and dissemination is an attractive aspect of this strategy.

Materials and methods

Mice

Male, 8–11-wk-old C57BL/6J mice and Thy1.1 C57BL/6J mice were obtained through a National Institute of Allergy and Infectious Diseases (NIAID) supply contract with Taconic Farms. All animal studies were conducted in Assessment and Accreditation of Laboratory Animal Care–accredited Biosafety Level 2 and 3 facilities at the NIAID/National Institutes of Health (NIH) by using a protocol (LPD-99E) approved by the NIAID Animal Care and Use Committee. Mice were housed under specific pathogen–free conditions with ad libitum access to food and water and were randomly assigned to experimental groups. All experiments were performed with either C57BL/6J or Thy1.1 C57BL/6J mice, which gave indistinguishable results.

Primary murine macrophages

Murine BMDMs were generated by the following procedure. Marrow from both femurs and tibiae was harvested in DMEM/F-12 (Gibco) supplemented with 10% heat-inactivated FBS (HyClone, Thermo Fisher Scientific) and flushed through a syringe with a 20-gauge needle. The dispersed cells were then seeded in Petri dishes (100 × 15 mm) containing 10 ml DMEM/F-12 supplemented with 2 mM L-glutamine (Gibco), 10% FBS, 2% Hepes (Life Technologies), 1 mM sodium pyruvate (Gibco), 25 µg/ml gentamicin (Gibco), and 20% of L929-conditioned media. After 3 d of incubation at 37°C with 5% CO_2, fresh medium containing L929-conditioned media without gentamicin was added. On day 6, macrophages were detached by the addition of cold Dulbecco's PBS (DPBS). The resulting cells were shown to be ∼95% pure based on extracellular double staining with anti-CD11b (eBioscience) and anti-F4/80 (BD Biosciences) macrophage markers by flow cytometric analysis.

Human monocyte–derived macrophages

$CD14^+$ column-purified human elutriated monocytes were obtained from peripheral blood of healthy donors from the NIH blood bank under Institutional Review Board–approved protocols of both the NIAID and the Department of Transfusion Medicine and were cultured in 96-well plates (Corning) in the presence of Roswell Park Memorial Institute (RPMI) 1640 media (Life Technologies) containing 10% human AB serum (Corning) and media containing growth factor (M-CSF) 50 ng/ml (PeproTech) for 7 d. Fresh M-CSF was added every 48 h, as previously described (Mayer-Barber et al., 2011). For in vitro experiments, the macrophages differentiated by this procedure were washed with 1× DPBS and cultured in the Opti-MEM media (Gibco) at 37°C in 5% CO_2 atmosphere. The resulting cells were shown to be ∼98% pure based on extracellular double staining with anti-$CD14^+$ (BD Biosciences) and anti-HLA-DR (BioLegend) macrophage markers and analyzed by flow cytometry.

Bacterial culture

Mtb H37Rv strain was grown in 7H9 broth (Sigma-Aldrich) supplemented with 0.05% Tween80 (Thermo Fisher Scientific), and 10% oleic acid–albumin-dextrose-catalase (OADC; BD Biosciences) at 37°C. Mtb H37Rv expressing the RFP, H37Rv-RFP, was kindly provided by Dr. Joel Ernst (University of California, San Francisco, San Francisco, CA) and grown in 7H9 broth supplemented with 0.05% Tween80, 10% OADC, and 30 µg/ml kanamycin (Sigma-Aldrich) at 37°C. Bacteria in mid-log phase (OD 0.6–1.0) were centrifuged at 5,000 revolutions per minute (rpm) for 10 min, resuspended in fresh 7H9 media, and frozen at −80°C in aliquots of ∼108 bacilli/ml.

In vitro macrophage infection

Prior to their use in in vitro experiments, bacterial aliquots were thawed, diluted in complete 7H9 broth media, and cultured at 37°C for 7 d. The bacterial concentration was then determined by spectrophotometry at 600 nm, centrifuged at 5,000 rpm for 10 min, and then resuspended in phenol and serum-free media (Opti-MEM). Bacteria were sonicated for 30 s and homogenized to reduce bacterial clumping.

BMDMs were exposed to H37Rv or H37Rv-RFP at the indicated MOI for 3 h, washed three times with 1× DPBS, and then cultured in fresh Opti-MEM media for 4 d. In some experiments, Fer-1 (Tocris) or PIH (Cayman Chemical) was added to the cultures 1 h before infection and then maintained in the same media for the entire experiment.

Measurement of cell death

Necrotic cell death was evaluated by staining adherent cells with either Live/Dead fixable blue dead cell stain kit (Invitrogen) or fixable viability dye (eBioscience) according to the manufacturer's protocol and as used previously in other studies of cell mortality (Downey et al., 2017; Zhao et al., 2017). Briefly, uninfected and infected cells were first stained with specific antibodies for CD11b (eBioscience) at 4°C for 30 min and then washed with 1× DPBS following centrifugation at 1,500 rpm for 5 min. Live/Dead staining solution (1:750 diluted in 1× DPBS) was added to the macrophage cultures, which were next incubated at room temperature for 15 min in the dark. The staining reaction was stopped by washing cells with 10% FBS in 1× DPBS and fixing them with cytofix/cytoperm buffer (BD Biosciences) at 4°C for ≥1 h. Macrophages were then detached, washed, resuspended in 1× DPBS with 1% BSA (MP Biomedicals) and analyzed by flow cytometry. Preliminary experiments confirmed that when high MFI of the dye is used as the readout, this assay measures death rather than unrelated cellular changes induced by Mtb infection (data not shown).

Cellular necrosis was also assessed by measuring the release of LDH in the supernatants from macrophage cultures with CytoTox 96 nonradioactive cytotoxicity assay (Promega) according to the manufacturer's instructions. In some experiments, annexin V staining was performed to evaluate apoptotic versus necrotic cell death in Mtb-infected macrophage cultures. Briefly, BMDMs were stained with Annexin V (BioLegend) diluted in annexin-binding buffer (BD Biosciences) for 20 min, washed with 1× DPBS, and then counterstained with anti-CD11b (eBioscience) and Live/Dead cell stain kit (Invitrogen). The samples were then analyzed by flow cytometry.

Bacterial enumeration

Live intracellular and extracellular CFU counts were determined at the indicated time points. Extracellular bacteria were

evaluated by plating serial dilutions of culture supernatants onto Middlebrook 7H11 (Sigma-Aldrich) agar plates supplemented with 0.5% (vol/vol) glycerol and 10% (vol/vol) OADC enrichment media. Total mycobacterial number (intracellular and extracellular) was assessed by performing CFU counts of whole BMDM cultures that were lysed with 0.05% saponin (Sigma-Aldrich) for 10 min. Colonies were counted after 21 d of incubation of 7H11 agar plates at 37°C.

Intracellular iron quantification

Labile intracellular iron was measured by using the calcein acetoxymethyl (AM) ester quenching method (Invitrogen) as previously described with some modifications (Picard et al., 1998; Thomas et al., 1999). Briefly, BMDMs were washed with 1× DPBS and lysed with 0.05% saponin for 10 min. Cell lysates were harvested, filter sterilized, and incubated with calcein AM (125 nM) at 37°C for 30 min. Duplicate samples were incubated with an iron chelator deferoxamine (Sigma-Aldrich) as a negative control, and cells treated with $FeSO_4$ (Sigma-Aldrich) were used as positive control. Calcein AM fluorescence was analyzed with a fluorescence microplate reader. Differential MFI of calcein AM between untreated and deferoxamine-treated samples was calculated to determine intracellular labile iron.

Mitochondrial superoxide assay

Mitochondrial superoxide was detected by using a flow cytometry–based assay. Macrophages were washed with 1× PBS to remove residual media and stained with MitoSOX probe (Life Technologies) at 37°C for 30 min following the manufacturer's protocol. Cells were next washed and fixed with cytofix/cytoperm at room temperature for 1 h. After fixation, cells were detached, washed, and resuspended in 1% BSA 1× DPBS. Fluorescence intensity of the probe was then measured in a flow cytometer.

Lipid peroxidation assay

Lipid peroxidation in macrophage cultures was assessed by using the Click-iT Lipid Peroxidation Imaging Kit (Life Technologies) or in the culture supernatants by using the TBARS assay kit (Cayman Chemical) according to the manufacturer's instructions. At the indicated time points, the culture supernatants were collected, filter sterilized, and assayed for the formation of malondialdehyde. The cellular monolayers were incubated with the LAA reagent (alkyne-modified linoleic acid) for detection of lipid peroxidation-derived protein modifications at 37°C for 1 h, and the cells were washed with 1× DPBS. After cell centrifugation (1,500 rpm for 5 min) to remove the LAA reagent, macrophages were stained for CD11b by using specific antibody at 4°C for 30 min. Live/Dead staining was performed as described previously above and the cells fixed by adding cytofix/cytoperm. Fixed cells were then detached, washed, and resuspended in 1× DPBS, and LAA fluorescence was analyzed by flow cytometry.

Measurement of intracellular GSH levels

At the indicated time points, BMDMs were washed with 1× DPBS, and then intracellular GSH levels were measured in cell lysates by using a Glutathione Assay Kit (Cayman Chemical) according to the manufacturer's instructions.

Western blotting

BMDMs were lysed with cell lysis buffer (Cell Signaling) supplemented with 2 mM PMSF (Sigma-Aldrich) and a complete Ultra protease inhibitor cocktail (Roche). Protein concentrations were determined by using Pierce 660-nm Protein Assay Reagent (Thermo Fisher Scientific) and normalized, and the protein samples were denatured by adding reducing buffer (Thermo Fisher Scientific) before incubation at 95°C for 5 min. Samples were separated in Mini-Protean TGX gels (Bio-Rad) and then transferred to the nitrocellulose membrane by using Trans-Blot Turbo Transfer System Bio-Rad machine according to manufacturer's instructions. Nitrocellulose membranes were blocked by using Odyssey blocking buffer (LI-COR) at room temperature for 2 h. Immunoblotting was performed by adding either anti-Gpx4 (1:1,000, clone EPNCIR144; Abcam) or anti-β actin (1:1,000, clone 8H10D10; Cell Signaling) and the membranes incubated at 4°C overnight. Subsequently, membranes were washed with 0.02% Tween20 (Sigma-Aldrich) in 1× DPBS and then treated with the respective secondary detection reagent (IRDye 800CW Donkey anti–rabbit IgG [LI-COR] or IRDye 680CW Donkey anti–mouse IgG [1:10,000; LI-COR]) at room temperature for 1 h. After washes in 0.02% DPBS-Tween20, membranes were imaged on a LI-COR Odyssey.

In vivo Mtb infection and treatment with Fer-1

8- to 11-wk-old male mice were used. Mice were infected either by intrapharyngeal or aerosol with the Mtb H37Rv strain (~10^3 CFU per mouse). A separate group of animals was used to determine bacterial intake by plating lung homogenates on Middlebrook 7H11 (Sigma-Aldrich) agar plates supplemented with 0.5% (vol/vol) glycerol (Mallinckrodt Pharmaceuticals) and 10% (vol/vol) OADC (BD Biosciences) enrichment media. In some experiments, mice received daily intraperitoneal injections of Fer-1 (3 mg/kg body weight) in 40% polyethyleneglycol-400 plus 0.3% DMSO or the vehicle alone starting at 15 d p.i.

Determination of mRNA expression

Total RNA was extracted from the lungs of Mtb-infected and uninfected naive mice by homogenizing the tissue in Trizol reagent (Life Technologies) and then by using the Direct-zol RNA Miniprep kit (Zymo Research) according to the manufacturer's instruction. cDNA was generated by reverse transcribing total RNA (1 µg of each RNA sample) by using SuperScript II reverse transcription and random primers (all from Invitrogen). Real-time quantitative PCR for several genes was performed on a 7900HT fast real-time PCR system (Applied Biosystems) by using SYBR Green PCR Master Mix (Applied Biosystems). GAPDH mRNA levels were used as a housekeeping gene to normalize mRNA levels. The relative mRNA expression of genes in Mtb-infected mouse lungs was calculated by using the $\Delta\Delta C_T$ (cycle threshold) method with further comparison of their expression in uninfected mouse lungs. The sequences of the specific primers are as follows: *gapdh*: forward, 5′-GGTGAAGGTCGG TGTGAAC-3′; reverse, 5′-CCATGTAGTTGAGGTCAATGAAGG-3′;

gpx4: forward, 5′-GCAACCAGTTTGGGAGGCAGGAG-3′; reverse, 5′-CCTCCATGGGACCATAGCGCTTC-3′; *slc7a11*: forward, 5′-CCTCTGCCAGCTGTTATTGTT-3′, reverse, 5′-CCTGGCAAAACTGAGGAAAT-3′.

Preparation of single-cell suspensions from lungs

Harvested lung lobes from infected and uninfected mice were washed with sterile 1× DPBS following organ dissection and then digested with collagenase IV (100 U/ml in RPMI; Sigma-Aldrich) at 37°C for 45 min under agitation (200 rpm). The enzymatic reaction was stopped by adding FBS. The pulmonary cells were dispersed by passage through a 100-µm pore-size cell strainer and red blood cells depleted by the addition of ammonium-chloride-potassium lysis buffer (Gibco) at room temperature for 2 min. Cells were next washed by centrifugation (1,200 rpm for 5 min) and cell pellets resuspended in RPMI supplemented with 10% FBS and 25 µg/ml gentamicin. The resulting cell preparations were counted and then seeded (8×10^4 cells/well) in round-bottom 96-well plates for LAA, as well as cell surface and Live/Dead staining.

Phenotypic analysis of lung infiltrating cells

Infiltrating cells in the lungs were stained by using appropriate combinations of directly conjugated or secondary antibodies. Antibodies used were directed against Ly6C (clone HK1.4), Ly6G (clone 1A8), CD11c (clone N418), F4/80 (clone BM8), CD45.2 (clone 104), CD45 (clone 30-F11), CD11b (clone M1/70), Syglec F (clone E50-2440), CD4 (clone GK1.5), CD8 (clone 53–6.7), Gpx4 (monoclonal rabbit unconjugated, clone EPNCIR144; Abcam). Unconjugated monoclonal rabbit antibody was detected with donkey F(ab′)2 anti–rabbit IgG H&L pre-adsorbed (ab181347; Abcam), and rabbit IgG monoclonal (ab172730; Abcam) was used as primary isotype control. Live/Dead fixable blue dead cell stain kit and Fixable Viability Dye eFluor 780 dye were purchased from Invitrogen Molecular Probes and eBioscience, respectively, and the staining was performed according to the manufacturer's specification. All samples were acquired on LSR Fortessa flow cytometer (BD Biosciences) and analyzed by using FlowJo 10.4.2 software (Tree Star).

In vivo determination of lipid peroxidation in lungs

Briefly, lungs were homogenized in 1× DPBS and centrifuged at 12,000 rpm at 4°C for 10 min to remove tissue matrix and cell debris. Supernatants were harvested, filter sterilized, and stored at −80°C. Lipid peroxidation was measured by using the TBARS assay kit (Cayman Chemical) according to the manufacturer's instructions.

Histopathology and necrotic tissue detection

The relative wet mass of each lung was determined by calculating the ratio of organ wet weight from infected mice and uninfected animals. Lungs were fixed with 10% formaldehyde, embedded in paraffin, sectioned, and stained with H&E dye to analyze tissue responses. Samples were examined under light microscopy with a Leica DMI6000 microscope and images acquired with a Leica DFC 425 color camera.

For detection of tissue necrosis, we used Sytox Green dye which stains exposed DNA that can then be visualized by fluorescence microscopy (Marques et al., 2015a,b). Briefly, we intravenously injected mice with 100 µl of a 50-µM solution of Sytox Green dye (Life Technologies) 20 min before mouse euthanasia. Lungs were then excised, washed with 1× DPBS, immediately fixed with 10% formaldehyde, and stored at 4°C for 48 h. Sytox Green fluorescence as the readout of tissue necrosis in whole-lung tissue was detected with a motorized stereomicroscope Leica M205 FA and images captured with a CFC345 cooled monochrome camera (Leica). Postacquisition images were processed by using LAS (Leica Application Suite) and Imaris 8.4.1 (Bitplane) software. Necrotic TB granuloma-like structures were defined manually based on fluorescence intensity and analyzed using ImageJ (NIH). Statistical analysis was performed using GraphPad Prism 7. Three lung lobes from three separate mice were analyzed per condition.

Determination of bacterial loads

CFU burden in the lung and spleen homogenates was assessed by serial dilutions and then plated onto 7H9 agar Petri dishes supplemented with 0.5% (vol/vol) glycerol and 10% (vol/vol) OADC enrichment media. Bacterial colonies were counted after 21 d of incubation at 37°C.

Statistics

All graphic data are presented as mean ± SEM values. For in vivo experiments, the sample size (n) is listed in the graphics of figure legends and indicates the number of animals per each experiment. For in vitro experiments, the number of experimental replicates is indicated in the figure legend. A single representative experiment is presented in the figures and the number of independent experiments performed is provided in the legends. Statistical analyses were performed with GraphPad Prism 7.0 software using either unpaired two-tailed t test for comparison between two groups or one-way ANOVA. Statistical differences were considered significant when $P < 0.05$ with asterisks denoting the degree of significance (*, $P < 0.05$; **, $P < 0.01$; ***, $P < 0.001$).

Online supplemental material

Fig. S1 shows that cell death occurring in Mtb-infected macrophages is nonapoptotic and caspase-1/11 independent. Fig. S2 displays a positive correlation between lipid peroxidation and cell death in Mtb-infected macrophages. Fig. S3 shows the association of enhanced superoxide production and lipid peroxidation with necrotic cell death in macrophage culture supplemented with iron. Fig. S4 shows that Fer-1 inhibits necrotic cell death under conditions of iron supplementation. Fig. S5 displays the effect of Fer-1 in human monocyte–derived macrophages infected with Mtb.

Acknowledgments

We are grateful to Sara Hieny, Sandra Oland, and the staff of the NIAID BSL2 and BSL3 animal facilities for their expert technical

assistance and thank Drs. Mahtab Moyeri and Dragana Jankovic for valuable discussion.

This work was supported by the Intramural Research Program, NIAID/NIH.

The authors declare no competing financial interests.

Author contributions: conceptualization, E.P. Amaral and A. Sher; methodology, E.P. Amaral, D.L. Costa, N. Riteau, O. Kamenyeva, L. Mittereder, K.D. Mayer-Barber, and B.B. Andrade; investigation, E.P. Amaral, D.L. Costa, S. Namasivayam, N. Riteau, and B.B. Andrade; resources, K.D. Mayer-Barber, B.B. Andrade, and A. Sher; writing (original draft), E.P. Amaral and A. Sher; writing (review and editing), E.P. Amaral, K.D. Mayer-Barber, B.B. Andrade, and A. Sher; supervision, A. Sher; funding acquisition, A. Sher.

Submitted: 17 September 2018
Revised: 15 December 2018
Accepted: 1 February 2019

References

Amaral, E.P., E.L. Conceição, D.L. Costa, M.S. Rocha, J.M. Marinho, M. Cordeiro-Santos, M.R. D'Império-Lima, T. Barbosa, A. Sher, and B.B. Andrade. 2016b. N-acetyl-cysteine exhibits potent anti-mycobacterial activity in addition to its known anti-oxidative functions. *BMC Microbiol.* 16:251. https://doi.org/10.1186/s12866-016-0872-7

Amaral, E.P., E.B. Lasunskaia, and M.R. D'Império-Lima. 2016a. Innate immunity in tuberculosis: how the sensing of mycobacteria and tissue damage modulates macrophage death. *Microbes Infect.* 18:11–20. https://doi.org/10.1016/j.micinf.2015.09.005

Andrade, B.B., N. Pavan Kumar, K.D. Mayer-Barber, D.L. Barber, R. Sridhar, V.V. Rekha, M.S. Jawahar, T.B. Nutman, A. Sher, and S. Babu. 2013. Plasma heme oxygenase-1 levels distinguish latent or successfully treated human tuberculosis from active disease. *PLoS One.* 8:e62618. https://doi.org/10.1371/journal.pone.0062618

Behar, S.M., M. Divangahi, and H.G. Remold. 2010. Evasion of innate immunity by *Mycobacterium tuberculosis*: is death an exit strategy? *Nat. Rev. Microbiol.* 8:668–674. https://doi.org/10.1038/nrmicro2387

Boelaert, J.R., S.J. Vandecasteele, R. Appelberg, and V.R. Gordeuk. 2007. The effect of the host's iron status on tuberculosis. *J. Infect. Dis.* 195: 1745–1753. https://doi.org/10.1086/518040

Boradia, V.M., H. Malhotra, J.S. Thakkar, V.A. Tillu, B. Vuppala, P. Patil, N. Sheokand, P. Sharma, A.S. Chauhan, M. Raje, and C.I. Raje. 2014. *Mycobacterium tuberculosis* acquires iron by cell-surface sequestration and internalization of human holo-transferrin. *Nat. Commun.* 5:4730. https://doi.org/10.1038/ncomms5730

Castillo, E.F., A. Dekonenko, J. Arko-Mensah, M.A. Mandell, N. Dupont, S. Jiang, M. Delgado-Vargas, G.S. Timmins, D. Bhattacharya, H. Yang, et al. 2012. Autophagy protects against active tuberculosis by suppressing bacterial burden and inflammation. *Proc. Natl. Acad. Sci. USA.* 109: E3168–E3176. https://doi.org/10.1073/pnas.1210500109

Chen, Y.L., X. Kong, Y. Xie, and R.C. Hider. 2018. The interaction of pyridoxal isonicotinoyl hydrazone (PIH) and salicylaldehyde isonicotinoyl hydrazone (SIH) with iron. *J. Inorg. Biochem.* 180:194–203. https://doi.org/10.1016/j.jinorgbio.2017.12.007

Conrad, M., V.E. Kagan, H. Bayir, G.C. Pagnussat, B. Head, M.G. Traber, and B. R. Stockwell. 2018. Regulation of lipid peroxidation and ferroptosis in diverse species. *Genes Dev.* 32:602–619. https://doi.org/10.1101/gad.314674.118

Costa, D.L., S. Namasivayam, E.P. Amaral, K. Arora, A. Chao, L.R. Mittereder, M. Maiga, H.I. Boshoff, C.E. Barry III, C.W. Goulding, et al. 2016. Pharmacological inhibition of host heme oxygenase-1 suppresses *Mycobacterium tuberculosis* infection in vivo by a mechanism dependent on T lymphocytes. *MBio.* 7:e01675-16. https://doi.org/10.1128/mBio.01675-16

Deshmukh, P., S. Unni, G. Krishnappa, and B. Padmanabhan. 2017. The Keap1-Nrf2 pathway: promising therapeutic target to counteract ROS-mediated damage in cancers and neurodegenerative diseases. *Biophys. Rev.* 9:41–56. https://doi.org/10.1007/s12551-016-0244-4

Divangahi, M., M. Chen, H. Gan, D. Desjardins, T.T. Hickman, D.M. Lee, S. Fortune, S.M. Behar, and H.G. Remold. 2009. *Mycobacterium tuberculosis* evades macrophage defenses by inhibiting plasma membrane repair. *Nat. Immunol.* 10:899–906. https://doi.org/10.1038/ni.1758

Divangahi, M., S.M. Behar, and H. Remold. 2013. Dying to live: how the death modality of the infected macrophage affects immunity to tuberculosis. *Adv. Exp. Med. Biol.* 783:103–120. https://doi.org/10.1007/978-1-4614-6111-1_6

Dixon, S.J., and B.R. Stockwell. 2014. The role of iron and reactive oxygen species in cell death. *Nat. Chem. Biol.* 10:9–17. https://doi.org/10.1038/nchembio.1416

Dixon, S.J., K.M. Lemberg, M.R. Lamprecht, R. Skouta, E.M. Zaitsev, C.E. Gleason, D.N. Patel, A.J. Bauer, A.M. Cantley, W.S. Yang, et al. 2012. Ferroptosis: an iron-dependent form of nonapoptotic cell death. *Cell.* 149:1060–1072. https://doi.org/10.1016/j.cell.2012.03.042

Dorhoi, A., and S.H. Kaufmann. 2016. Pathology and immune reactivity: understanding multidimensionality in pulmonary tuberculosis. *Semin. Immunopathol.* 38:153–166. https://doi.org/10.1007/s00281-015-0531-3

Downey, J., E. Pernet, F. Coulombe, B. Allard, I. Meunier, J. Jaworska, S. Qureshi, D.C. Vinh, J.G. Martin, P. Joubert, and M. Divangahi. 2017. RIPK3 interacts with MAVS to regulate type I IFN-mediated immunity to Influenza A virus infection. *PLoS Pathog.* 13:e1006326. https://doi.org/10.1371/journal.ppat.1006326

Dragset, M.S., G. Poce, S. Alfonso, T. Padilla-Benavides, T.R. Ioerger, T. Kaneko, J.C. Sacchettini, M. Biava, T. Parish, J.M. Argüello, et al. 2015. A novel antimycobacterial compound acts as an intracellular iron chelator. *Antimicrob. Agents Chemother.* 59:2256–2264. https://doi.org/10.1128/AAC.05114-14

Elkington, P.T., J.M. D'Armiento, and J.S. Friedland. 2011. Tuberculosis immunopathology: the neglected role of extracellular matrix destruction. *Sci. Transl. Med.* 3:71ps6. https://doi.org/10.1126/scitranslmed.3001847

Gangaidzo, I.T., V.M. Moyo, E. Mvundura, G. Aggrey, N.L. Murphree, H. Khumalo, T. Saungweme, I. Kasvosve, Z.A. Gomo, T. Rouault, et al. 2001. Association of pulmonary tuberculosis with increased dietary iron. *J. Infect. Dis.* 184:936–939. https://doi.org/10.1086/323203

Gordeuk, V.R., C.E. McLaren, A.P. MacPhail, G. Deichsel, and T.H. Bothwell. 1996. Associations of iron overload in Africa with hepatocellular carcinoma and tuberculosis: Strachan's 1929 thesis revisited. *Blood.* 87: 3470–3476.

Gutierrez, M.G., S.S. Master, S.B. Singh, G.A. Taylor, M.I. Colombo, and V. Deretic. 2004. Autophagy is a defense mechanism inhibiting BCG and *Mycobacterium tuberculosis* survival in infected macrophages. *Cell.* 119: 753–766. https://doi.org/10.1016/j.cell.2004.11.038

Harvey, C.J., R.K. Thimmulappa, A. Singh, D.J. Blake, G. Ling, N. Wakabayashi, J. Fujii, A. Myers, and S. Biswal. 2009. Nrf2-regulated glutathione recycling independent of biosynthesis is critical for cell survival during oxidative stress. *Free Radic. Biol. Med.* 46:443–453. https://doi.org/10.1016/j.freeradbiomed.2008.10.040

Hermes-Lima, M., N.C. Santos, J. Yan, M. Andrews, H.M. Schulman, and P. Ponka. 1999. EPR spin trapping and 2-deoxyribose degradation studies of the effect of pyridoxal isonicotinoyl hydrazone (PIH) on *OH formation by the Fenton reaction. *Biochim. Biophys. Acta.* 1426:475–482. https://doi.org/10.1016/S0304-4165(98)00167-6

Hermes-Lima, M., P. Ponka, and H.M. Schulman. 2000. The iron chelator pyridoxal isonicotinoyl hydrazone (PIH) and its analogues prevent damage to 2-deoxyribose mediated by ferric iron plus ascorbate. *Biochim. Biophys. Acta.* 1523:154–160. https://doi.org/10.1016/S0304-4165(00)00115-X

Hernández, J., A. Garibay-Escobar, A. Mendoza-Mendoza, A. Pinelli-Saavedra, and O. Valenzuela. 2008. Effect of exogenous vitamin E on proliferation and cytokine production in peripheral blood mononuclear cells from patients with tuberculosis. *Br. J. Nutr.* 99:224–229. https://doi.org/10.1017/S0007114507795302

Hou, W., Y. Xie, X. Song, X. Sun, M.T. Lotze, H.J. Zeh III, R. Kang, and D. Tang. 2016. Autophagy promotes ferroptosis by degradation of ferritin. *Autophagy.* 12:1425–1428. https://doi.org/10.1080/15548627.2016.1187366

Ingold, I., C. Berndt, S. Schmitt, S. Doll, G. Poschmann, K. Buday, A. Roveri, X. Peng, F. Porto Freitas, T. Seibt, et al. 2018. Selenium Utilization by GPX4 Is Required to Prevent Hydroperoxide-Induced Ferroptosis. *Cell.* 172: 409–422.e21. https://doi.org/10.1016/j.cell.2017.11.048

Jorgensen, I., M. Rayamajhi, and E.A. Miao. 2017. Programmed cell death as a defence against infection. *Nat. Rev. Immunol.* 17:151–164. https://doi.org/10.1038/nri.2016.147

Kang, R., L. Zeng, S. Zhu, Y. Xie, J. Liu, Q. Wen, L. Cao, M. Xie, Q. Ran, G. Kroemer, et al. 2018. Lipid Peroxidation Drives Gasdermin D-Mediated

Pyroptosis in Lethal Polymicrobial Sepsis. *Cell Host Microbe.* 24:97–108. e4. https://doi.org/10.1016/j.chom.2018.05.009

Kaplan, G., F.A. Post, A.L. Moreira, H. Wainwright, B.N. Kreiswirth, M. Tanverdi, B. Mathema, S.V. Ramaswamy, G. Walther, L.M. Steyn, et al. 2003. *Mycobacterium tuberculosis* growth at the cavity surface: a microenvironment with failed immunity. *Infect. Immun.* 71:7099–7108. https://doi.org/10.1128/IAI.71.12.7099-7108.2003

Kiran, D., B.K. Podell, M. Chambers, and R.J. Basaraba. 2016. Host-directed therapy targeting the *Mycobacterium tuberculosis* granuloma: a review. *Semin. Immunopathol.* 38:167–183. https://doi.org/10.1007/s00281-015-0537-x

Lee, J., T. Repasy, K. Papavinasasundaram, C. Sassetti, and H. Kornfeld. 2011. *Mycobacterium tuberculosis* induces an atypical cell death mode to escape from infected macrophages. *PLoS One.* 6:e18367. https://doi.org/10.1371/journal.pone.0018367

Lemire, J.A., J.J. Harrison, and R.J. Turner. 2013. Antimicrobial activity of metals: mechanisms, molecular targets and applications. *Nat. Rev. Microbiol.* 11:371–384. https://doi.org/10.1038/nrmicro3028

Lerner, T.R., S. Borel, D.J. Greenwood, U. Repnik, M.R. Russell, S. Herbst, M. L. Jones, L.M. Collinson, G. Griffiths, and M.G. Gutierrez. 2017. *Mycobacterium tuberculosis* replicates within necrotic human macrophages. *J. Cell Biol.* 216:583–594. https://doi.org/10.1083/jcb.201603040

Linkermann, A., R. Skouta, N. Himmerkus, S.R. Mulay, C. Dewitz, F. De Zen, A. Prokai, G. Zuchtriegel, F. Krombach, P.S. Welz, et al. 2014a. Synchronized renal tubular cell death involves ferroptosis. *Proc. Natl. Acad. Sci. USA.* 111:16836–16841. https://doi.org/10.1073/pnas.1415518111

Linkermann, A., B.R. Stockwell, S. Krautwald, and H.J. Anders. 2014b. Regulated cell death and inflammation: an auto-amplification loop causes organ failure. *Nat. Rev. Immunol.* 14:759–767. https://doi.org/10.1038/nri3743

Lounis, N., C. Maslo, J.R. Boelaert, P. Bonnafous, C. Trnffot-Pernot, J. Baohong, and J. Grosset. 1999. Impact of iron loading and iron chelation on murine tuberculosis. *Clin. Microbiol. Infect.* 5:687–692. https://doi.org/10.1111/j.1469-0691.1999.tb00514.x

Lounis, N., C. Truffot-Pernot, J. Grosset, V.R. Gordeuk, and J.R. Boelaert. 2001. Iron and *Mycobacterium tuberculosis* infection. *J. Clin. Virol.* 20:123–126. https://doi.org/10.1016/S1386-6532(00)00136-0

Mancias, J.D., X. Wang, S.P. Gygi, J.W. Harper, and A.C. Kimmelman. 2014. Quantitative proteomics identifies NCOA4 as the cargo receptor mediating ferritinophagy. *Nature.* 509:105–109. https://doi.org/10.1038/nature13148

Marques, P.E., M.M. Antunes, B.A. David, R.V. Pereira, M.M. Teixeira, and G. B. Menezes. 2015a. Imaging liver biology in vivo using conventional confocal microscopy. *Nat. Protoc.* 10:258–268. https://doi.org/10.1038/nprot.2015.006

Marques, P.E., A.G. Oliveira, R.V. Pereira, B.A. David, L.F. Gomides, A.M. Saraiva, D.A. Pires, J.T. Novaes, D.O. Patricio, D. Cisalpino, et al. 2015b. Hepatic DNA deposition drives drug-induced liver injury and inflammation in mice. *Hepatology.* 61:348–360. https://doi.org/10.1002/hep.27216

Martin, C.J., M.G. Booty, T.R. Rosebrock, C. Nunes-Alves, D.M. Desjardins, I. Keren, S.M. Fortune, H.G. Remold, and S.M. Behar. 2012. Efferocytosis is an innate antibacterial mechanism. *Cell Host Microbe.* 12:289–300. https://doi.org/10.1016/j.chom.2012.06.010

Mayer-Barber, K.D., B.B. Andrade, D.L. Barber, S. Hieny, C.G. Feng, P. Caspar, S. Oland, S. Gordon, and A. Sher. 2011. Innate and adaptive interferons suppress IL-1α and IL-1β production by distinct pulmonary myeloid subsets during Mycobacterium tuberculosis infection. *Immunity.* 35: 1023–1034. https://doi.org/10.1016/j.immuni.2011.12.002

Meyer, D. 2006. Iron chelation as therapy for HIV and *Mycobacterium tuberculosis* co-infection under conditions of iron overload. *Curr. Pharm. Des.* 12:1943–1947. https://doi.org/10.2174/138161206777442164

Molloy, A., P. Laochumroonvorapong, and G. Kaplan. 1994. Apoptosis, but not necrosis, of infected monocytes is coupled with killing of intracellular bacillus Calmette-Guérin. *J. Exp. Med.* 180:1499–1509. https://doi.org/10.1084/jem.180.4.1499

Moraco, A.H., and H. Kornfeld. 2014. Cell death and autophagy in tuberculosis. *Semin. Immunol.* 26:497–511. https://doi.org/10.1016/j.smim.2014.10.001

Newton, K., D.L. Dugger, K.E. Wickliffe, N. Kapoor, M.C. de Almagro, D. Vucic, L. Komuves, R.E. Ferrando, D.M. French, J. Webster, et al. 2014. Activity of protein kinase RIPK3 determines whether cells die by necroptosis or apoptosis. *Science.* 343:1357–1360. https://doi.org/10.1126/science.1249361

Oddo, M., T. Renno, A. Attinger, T. Bakker, H.R. MacDonald, and P.R. Meylan. 1998. Fas ligand-induced apoptosis of infected human macrophages reduces the viability of intracellular *Mycobacterium tuberculosis*. *J. Immunol.* 160:5448–5454.

Owens, C.P., N. Chim, and C.W. Goulding. 2013. Insights on how the *Mycobacterium tuberculosis* heme uptake pathway can be used as a drug target. *Future Med. Chem.* 5:1391–1403. https://doi.org/10.4155/fmc.13.109

Pajuelo, D., N. Gonzalez-Juarbe, U. Tak, J. Sun, C.J. Orihuela, and M. Niederweis. 2018. NAD^+ Depletion Triggers Macrophage Necroptosis, a Cell Death Pathway Exploited by Mycobacterium tuberculosis. *Cell Reports.* 24:429–440. https://doi.org/10.1016/j.celrep.2018.06.042

Pan, H., B.S. Yan, M. Rojas, Y.V. Shebzukhov, H. Zhou, L. Kobzik, D.E. Higgins, M.J. Daly, B.R. Bloom, and I. Kramnik. 2005. Ipr1 gene mediates innate immunity to tuberculosis. *Nature.* 434:767–772. https://doi.org/10.1038/nature03419

Pasparakis, M., and P. Vandenabeele. 2015. Necroptosis and its role in inflammation. *Nature.* 517:311–320. https://doi.org/10.1038/nature14191

Picard, V., S. Epsztejn, P. Santambrogio, Z.I. Cabantchik, and C. Beaumont. 1998. Role of ferritin in the control of the labile iron pool in murine erythroleukemia cells. *J. Biol. Chem.* 273:15382–15386. https://doi.org/10.1074/jbc.273.25.15382

Reddy, V.P., K.C. Chinta, V. Saini, J.N. Glasgow, T.D. Hull, A. Traylor, F. Rey-Stolle, M.P. Soares, R. Madansein, M.A. Rahman, et al. 2018. Ferritin H deficiency in myeloid compartments dysregulates host energy metabolism and increases susceptibility to *Mycobacterium tuberculosis* infection. *Front. Immunol.* 9:860. https://doi.org/10.3389/fimmu.2018.00860

Riendeau, C.J., and H. Kornfeld. 2003. THP-1 cell apoptosis in response to Mycobacterial infection. *Infect. Immun.* 71:254–259. https://doi.org/10.1128/IAI.71.1.254-259.2003

Schaible, U.E., H.L. Collins, F. Priem, and S.H. Kaufmann. 2002. Correction of the iron overload defect in beta-2-microglobulin knockout mice by lactoferrin abolishes their increased susceptibility to tuberculosis. *J. Exp. Med.* 196:1507–1513. https://doi.org/10.1084/jem.20020897

Seyedrezazadeh, E., A. Ostadrahimi, S. Mahboob, Y. Assadi, J. Ghaemmagami, and M. Pourmogaddam. 2008. Effect of vitamin E and selenium supplementation on oxidative stress status in pulmonary tuberculosis patients. *Respirology.* 13:294–298. https://doi.org/10.1111/j.1440-1843.2007.01200.x

Shiloh, M.U., P. Manzanillo, and J.S. Cox. 2008. *Mycobacterium tuberculosis* senses host-derived carbon monoxide during macrophage infection. *Cell Host Microbe.* 3:323–330. https://doi.org/10.1016/j.chom.2008.03.007

Silva-Gomes, S., S. Vale-Costa, R. Appelberg, and M.S. Gomes. 2013. Iron in intracellular infection: to provide or to deprive? *Front. Cell. Infect. Microbiol.* 3:96. https://doi.org/10.3389/fcimb.2013.00096

Skouta, R., S.J. Dixon, J. Wang, D.E. Dunn, M. Orman, K. Shimada, P.A. Rosenberg, D.C. Lo, J.M. Weinberg, A. Linkermann, and B.R. Stockwell. 2014. Ferrostatins inhibit oxidative lipid damage and cell death in diverse disease models. *J. Am. Chem. Soc.* 136:4551–4556. https://doi.org/10.1021/ja411006a

Stockwell, B.R., J.P. Friedmann Angeli, H. Bayir, A.I. Bush, M. Conrad, S.J. Dixon, S. Fulda, S. Gascón, S.K. Hatzios, V.E. Kagan, et al. 2017. Ferroptosis: A regulated cell death nexus linking metabolism, redox biology, and disease. *Cell.* 171:273–285. https://doi.org/10.1016/j.cell.2017.09.021

Stutz, M.D., S. Ojaimi, C. Allison, S. Preston, P. Arandjelovic, J.M. Hildebrand, J.J. Sandow, A.I. Webb, J. Silke, W.S. Alexander, and M. Pellegrini. 2018a. Necroptotic signaling is primed in *Mycobacterium tuberculosis*-infected macrophages, but its pathophysiological consequence in disease is restricted. *Cell Death Differ.* 25:951–965. https://doi.org/10.1038/s41418-017-0031-1

Stutz, M.D., S. Ojaimi, G. Ebert, and M. Pellegrini. 2018b. Is receptor-interacting protein kinase 3 a viable therapeutic target for *Mycobacterium tuberculosis* infection? *Front. Immunol.* 9:1178. https://doi.org/10.3389/fimmu.2018.01178

Su, L., B. Quade, H. Wang, L. Sun, X. Wang, and J. Rizo. 2014. A plug release mechanism for membrane permeation by MLKL. *Structure.* 22: 1489–1500. https://doi.org/10.1016/j.str.2014.07.014

Tanzer, M.C., A. Tripaydonis, A.I. Webb, S.N. Young, L.N. Varghese, C. Hall, W.S. Alexander, J.M. Hildebrand, J. Silke, and J.M. Murphy. 2015. Necroptosis signalling is tuned by phosphorylation of MLKL residues outside the pseudokinase domain activation loop. *Biochem. J.* 471: 255–265. https://doi.org/10.1042/BJ20150678

Thomas, F., G. Serratrice, C. Béguin, E.S. Aman, J.L. Pierre, M. Fontecave, and J.P. Laulhère. 1999. Calcein as a fluorescent probe for ferric iron. Application to iron nutrition in plant cells. *J. Biol. Chem.* 274:13375–13383. https://doi.org/10.1074/jbc.274.19.13375

Toyokuni, S., F. Ito, K. Yamashita, Y. Okazaki, and S. Akatsuka. 2017. Iron and thiol redox signaling in cancer: An exquisite balance to escape ferroptosis. *Free Radic. Biol. Med.* 108:610–626. https://doi.org/10.1016/j.freeradbiomed.2017.04.024

Trousseau, A. 1872. True, false chlorosis. *In Lectures on clinical medicine.* The New Sydenham Society, London. pp. 95–117.

Venketaraman, V., A. Millman, M. Salman, S. Swaminathan, M. Goetz, A. Lardizabal, David Hom, and N.D. Connell. 2008. Glutathione levels and immune responses in tuberculosis patients. *Microb. Pathog.* 44:255–261. https://doi.org/10.1016/j.micpath.2007.09.002

Vilchèze, C., T. Hartman, B. Weinrick, and W.R. Jacobs Jr. 2013. *Mycobacterium tuberculosis* is extraordinarily sensitive to killing by a vitamin C-induced Fenton reaction. *Nat. Commun.* 4:1881. https://doi.org/10.1038/ncomms2898

Wallis, R.S., and R. Hafner. 2015. Advancing host-directed therapy for tuberculosis. *Nat. Rev. Immunol.* 15:255–263. https://doi.org/10.1038/nri3813

Weinlich, R., A. Oberst, H.M. Beere, and D.R. Green. 2017. Necroptosis in development, inflammation and disease. *Nat. Rev. Mol. Cell Biol.* 18:127–136. https://doi.org/10.1038/nrm.2016.149

Welin, A., D. Eklund, O. Stendahl, and M. Lerm. 2011. Human macrophages infected with a high burden of ESAT-6-expressing *M. tuberculosis* undergo caspase-1- and cathepsin B-independent necrosis. *PLoS One.* 6:e20302. https://doi.org/10.1371/journal.pone.0020302

Wong, K.W., and W.R. Jacobs Jr. 2011. Critical role for NLRP3 in necrotic death triggered by *Mycobacterium tuberculosis*. *Cell. Microbiol.* 13:1371–1384. https://doi.org/10.1111/j.1462-5822.2011.01625.x

World Health Organization. 2017. *World Health Organization. Tuberculosis Fact Sheet. Number 104.* World Health Organization, Geneva.

Zhao, X., N. Khan, H. Gan, F. Tzelepis, T. Nishimura, S.Y. Park, M. Divangahi, and H.G. Remold. 2017. Bcl-x_L mediates RIPK3-dependent necrosis in M. tuberculosis-infected macrophages. *Mucosal Immunol.* 10:1553–1568. https://doi.org/10.1038/mi.2017.12